Asian Journal of Periodontics and Orthodontics

2025, Volume 5, Page No: 73-84 Copyright CC BY-NC-SA 4.0 Available online at: <u>www.tsdp.net</u>



Original Article

Periodontal Gap Dynamics after Prolonged Tooth Movement into Surgically Augmented Critical-Size Defects in Beagle Jaws

Ajay Pal¹*, Lynn Wilhelmy², Christina Maria Liebl¹, Chandran Mas³, Benedict Wilmes¹

¹Department of Orthodontics, Rostock University Medical Centre, 18057 Rostock, Germany.

²Working Group for Implant Materials, Faculty of Mechanical Engineering and Marine Technology, University of Rostock, 18119 Rostock, Germany.

³Department of Oral and Maxillofacial Surgery, Rostock University Medical Centre, 18057 Rostock, Germany.

*E-mail ⊠ Palajay.de@yahoo.com

Received: 11 March 2025; Revised: 25 June 2025; Accepted: 25 June 2025

ABSTRACT

Orthodontic tooth movement triggers complex and coordinated remodeling within the periodontal ligament (PDL) and adjacent alveolar bone. In certain clinical situations, such as cleft lip, alveolus, and palate cases, teeth must be guided into surgically augmented bone defects. Although the role of the PDL in tooth displacement is recognized, its response under these conditions is not completely clarified. This study evaluated the PDL after 23 weeks of tooth movement into critical-sized augmented defects. In four beagle dogs, second molars were orthodontically moved into critical-sized defects filled with bovine xenograft or nanocrystalline hydroxyapatite, with autogenous bone as the control. After 23 weeks, histological samples were examined under the microscope, and PDL dimensions were measured. Statistical analysis was conducted using the Wilcoxon–Mann–Whitney test. Across all graft materials, the PDL was consistently wider on the tension side than on the compression side (p \leq 0.05), for both mesial and distal roots. By 23 weeks, PDL remodeling had stabilized, producing a wider ligament on the tension side, in contrast to the initial response observed shortly after force application.

Keywords: Periodontal ligament, Bone grafting materials, Orthodontic tooth movement, Alveolar bone repair **How to Cite This Article:** Pal A, Wilhelmy L, Liebl CM, Mas C, Wilmes B. Periodontal Gap Dynamics after Prolonged Tooth Movement into Surgically Augmented Critical-Size Defects in Beagle Jaws. Asian J Periodont Orthodont. 2025;5:73-84. https://doi.org/10.51847/cVs4fa5Szy

Introduction

Orthodontic tooth movement is facilitated by a sequence of precisely coordinated cellular events and signaling pathways triggered by controlled mechanical forces [1]. Bone remodeling, which involves osteoblasts, osteoclasts, and osteocytes, follows the Biphasic Theory, wherein the Catabolic Phase occurs on the compression side prior to the Anabolic Phase on the tension side of the tooth root [2]. During this process, the periodontal ligament (PDL) undergoes compression on the side toward the direction of tooth displacement and stretching on the opposite side [3–5]. Although the detailed mechanisms remain

incompletely understood [6], the PDL's critical function in bone remodeling during tooth movement has been firmly established [7].

The application of orthodontic forces triggers a sterile inflammatory response [2, 5], promoting remodeling of both the PDL [8] and alveolar bone [2]. The PDL maintains the optimal spacing between the tooth and surrounding bone, allowing effective transmission of mechanical forces [9]. Significant dimensional changes in the PDL occur during tooth movement, which differ between the compression and tension sides. Studies in rodents consistently report narrowing of the PDL on the compression side and widening on the tension side

[5, 10–15], with comparisons to untreated controls confirming expansion of the PDL on the tension side [5, 12, 14]. These changes are most pronounced during the initial 1–14 days after force application. For example, in rats, Tsuge *et al.* observed a 24-hour increase in PDL width on the tension side, returning to near-baseline within seven days [5]. Laura *et al.* described similar 14-day trends in both normal and diabetic rats treated with insulin alone or in combination with metformin [13].

Long-term observations are rarer. Rizk *et al.* tracked orthodontic tooth movement and alveolar bone remodeling in mice over five weeks using high-resolution micro-CT, reporting greater PDL thickness around moved teeth compared to controls, although differentiating compression from tension sides in small animals proved challenging [9].

The dynamics of tooth movement into augmented bone are still under debate. Sun *et al.* demonstrated that reconstructions using iliac crest autografts stimulate bone remodeling [16]. Ru *et al.* compared bovine xenografts with synthetic beta-tricalcium phosphate/hydroxyapatite mixtures, finding slower tooth movement and reduced root resorption with the synthetic combination [17]. Another rat study comparing autologous bone, human xenografts, and a beta-tricalcium phosphate/hydroxyapatite composite

over 57 days found similar tooth movement distances across groups [18].

This study examined PDL changes in beagle dogs after 23 weeks of orthodontic movement into critical-sized defects. This extended period simulates clinical scenarios, as early days and weeks show pronounced PDL remodeling. The main goal was to assess the dimensional changes of the PDL on the compression and tension sides of orthodontically moved tooth roots over this long-term period.

Materials and Methods

A prospective in vivo study was designed using beagle dogs to investigate periodontal ligament (PDL) adaptations following prolonged orthodontic tooth movement into grafted mandibular defects. Critical-sized defects (CSDs)—defined as bone defects that do not spontaneously heal [19]—were filled with autologous bone or two alternative bone replacement materials (BRMs). The second premolars (PM2) adjacent to the defects were orthodontically moved into the grafted regions. After a 23-week period, PDL dimensions surrounding PM2 were histologically assessed. A schematic timeline of the experimental procedure is presented in Figure 1.

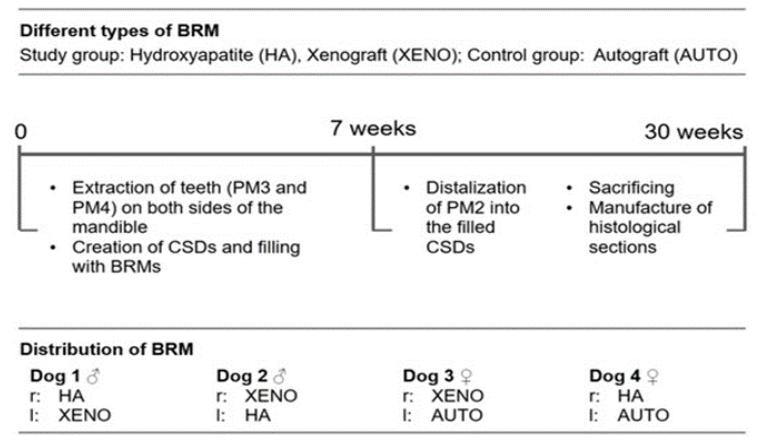


Figure 1. Schematic of the experimental design illustrating critical-sized mandibular defects in four beagle dogs filled with autograft (AUTO), bovine xenograft (XENO), or nanocrystalline hydroxyapatite (HA). Abbreviations: CSD = critical-sized defect; PM = premolar; r = right mandibular side; l = left mandibular side; HA = hydroxyapatite; XENO = xenograft; AUTO = autograft.

Surgical procedure and orthodontic setup Animals

Four beagle dogs (2 males, 2 females; BASF, Ludwigshafen, Germany) were included. All procedures followed ARRIVE guidelines, and ethics approval is detailed in the Supplementary Materials. Following surgery, animals were maintained on a soft diet with ad libitum water access. Anesthesia was

induced with premedication using acepromazine (10 mg/mL, 0.2 mL per 10 kg body weight) and L-polamivet (1.0 mL per 10 kg body weight). Propofol (10 mg/mL, 3–4 mg/kg) was used to achieve anesthesia, which was maintained with 1.1–1.8 Vol% isoflurane in oxygen. Animals were gradually awakened by stopping isoflurane administration.

Experimental design

Critical-sized defects (Table 1) were created at the superior border of the mandibular alveolar process immediately after extraction of PM3 and PM4. The control group (AUTO) received autologous bone, while experimental groups were grafted with either nanocrystalline hydroxyapatite (NanoBone®, Artoss GmbH, Rostock, Germany; HA) or deproteinized bovine bone mineral (BioOss®, Geistlich Pharma, Wolhusen, Switzerland; XENO). Material assignment was randomized with assistance from the Institute for

Biostatistics and Informatics in Medicine and Ageing Research, University Medical Centre, Rostock, Germany. All grafts were stabilized using 2.0 Miniplate osteosynthesis (MPOS; Mondeal Company, Mühlheim, Germany) (Figure 2a). Two mini-screws were inserted anteriorly in the mandible to enable subsequent orthodontic tooth movement. Dental radiographs were acquired using the HF3000 X-ray system (Gierth X-Ray International GmbH, Riesa, Germany) to verify placement and graft stabilization (Figures 2b–2d).

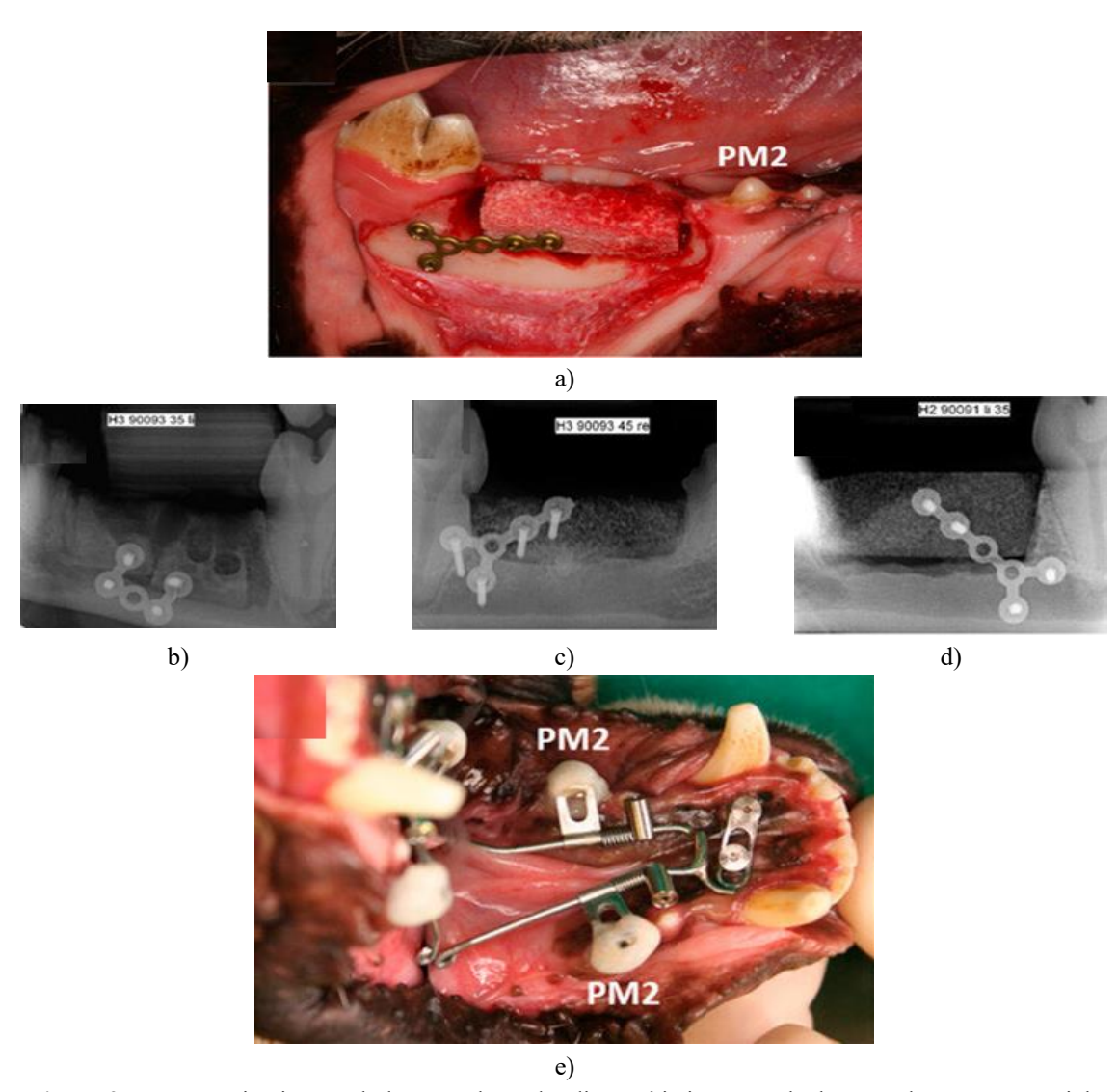


Figure 2. Postoperative intraoral photographs and radiographic images. The bone replacement materials (BRMs) were secured distal to the second premolar (PM2) (a). Radiographs obtained immediately after surgery display the autograft (b), xenograft (c), and hydroxyapatite (d). Seven weeks following BRM placement, PM2 was distally moved bilaterally using a skeletal-anchored orthodontic device, corresponding to the Beneslider system (e).

Table 1. Dimensions of all critical-sized defects in millimeters (length \times height \times depth).

Jaw Side	Dog 1	Dog 2	Dog 3	Dog 4	
Right Side	$29 \times 9 \times 10$	$26 \times 9 \times 8$	$24 \times 9 \times 10$	$26 \times 9 \times 8$	

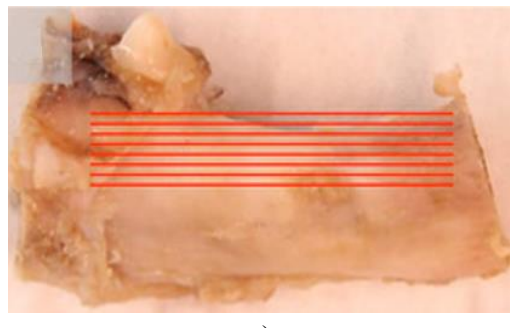
A second surgical session was conducted seven weeks after BRM implantation, adhering to the previously described anesthesia protocol. Bilateral distalization of PM2 into the augmented sites was initiated using custom orthodontic appliances with skeletal anchorage (Figure 2e). These devices (Beneslider system, Benefit-System, PSM Medical Solutions, Tuttlingen, Germany) were activated with a maximum load of 240 g and were not readjusted during the 23-week experimental period. Upon completion, the animals were euthanized, and mandibles were harvested and preserved in artificial saliva (DAC/RF 7.5) supplemented with 2.5% glutardialdehyde until histomorphometric preparation.

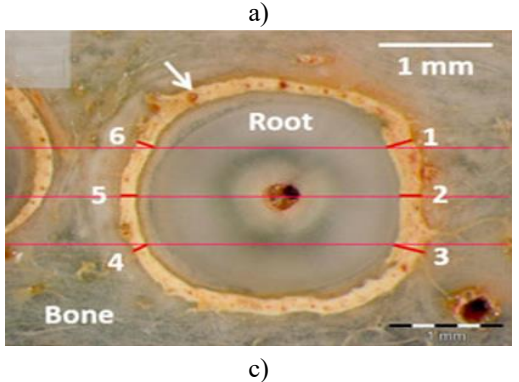
Histomorphometric preparation, data collection, and analysis

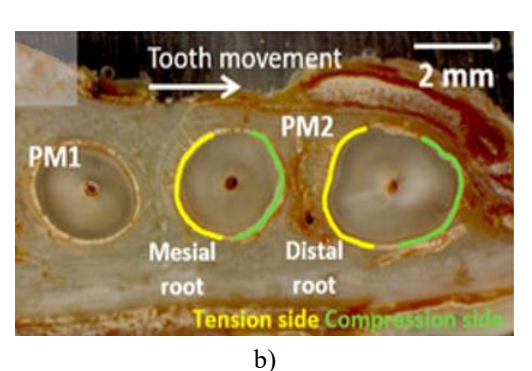
The excised mandibles (n = 3) were embedded in coldcuring epoxy resin at 4 °C (EpoThin resin and hardener, Buehler, Germany). Cross-sectional slices of 1 mm thickness were prepared using a HistoSaw® DDM-P 216 (Medim, Giessen, Germany) under continuous water cooling. Each slice was subsequently ground to a thickness of 20 μm (Tegra-Pol-15, Stuers, Willich, Germany) employing silicon carbide wet grinding paper (Buehler, Düsseldorf, Germany) with sequential grain sizes ranging from P-500 to P-4000. Following unstained examination, slices were stained sequentially with toluidine blue and azure eosin: 30 minutes in toluidine blue (Sigma Aldrich Chemie GmbH, Darmstadt, Germany), rinsed with distilled water, dehydrated in 100% ethanol, followed by 20 minutes in azure eosin (Merck, Darmstadt, Germany), rinsed again, and dehydrated. Light microscopy (SZX10, Olympus Germany, Hamburg, Germany) and scanning acoustic microscopy (SAM 300, PVA TePla GmbH, Wettenberg, Germany) were used for imaging. Ultrasound C-scans were obtained from the surface of each slice using a single-element 100 MHz ultrasound transducer in a water bath.

Periodontal gap assessment

Unstained sections (Figure 3a) were utilized to quantify PDL widths around the mesial and distal roots of PM2. Measurements distinguished between the compression side (toward the OTM) and the tension side (opposite the OTM) (Figure 3b). The periodontal gap was defined as the distance from the root surface (cementum) to the alveolar bone (Figures 3c and 3d). PDL widths were measured at three points per side (points 1–6 in Figures 3c and 3d) using Gimp 2.10.6, with horizontal lines spaced 500 µm apart and aligned to the root canal center. LM and SAM imaging clearly distinguished the boundaries between bone, PDL, and tooth. Analyses were performed using both LM (Figure 3c) and SAM (Figure 3d) images.







Bone 1 mm

Root 1

5 2

4 3

76

Figure 3. Mandible after resection, displaying the selected slicing planes (a). Panel (b) illustrates a cross-section containing the first premolar (PM1) root and the mesial and distal roots of the second premolar (PM2), which was orthodontically moved into the filled critical-sized defect. Based on the direction of tooth movement, yellow lines designate the tension side, while green lines denote the compression side of PM2 roots. Light microscopy (c) and scanning acoustic microscopy (d) images focus on the distal PM2 root located within the augmented critical-sized defect (Dog 3, left side). Arrows indicate the periodontal ligament gaps measured at three points on the compression side (1–3) and three points on the tension side (4–6).

Quantification of bone, osteoid, and bone marrow
Stained sections were used to determine the relative
proportions of mineralized bone, osteoid/cartilage
matrix, and bone marrow. For image selection, the
following criteria were applied: (a) section located
above the mandibular canal, (b) PM2 root included, (c)
alveolar bone present distal to the root. Three to five
images per section were manually combined to create
a panoramic view encompassing PM2 and at least 20

mm in the distal direction (**Figure 4**). Two polygonal regions of interest (ROIs) were defined: the mesial ROI started 10 mm behind the PM2 root, while the distal ROI continued without a gap for another 10 mm, encompassing the original critical-sized defect. Distinct reflection signals allowed differentiation of mineralized bone (blue/phase A), osteoid/cartilage matrix (green/phase B), and bone marrow (red/phase C).

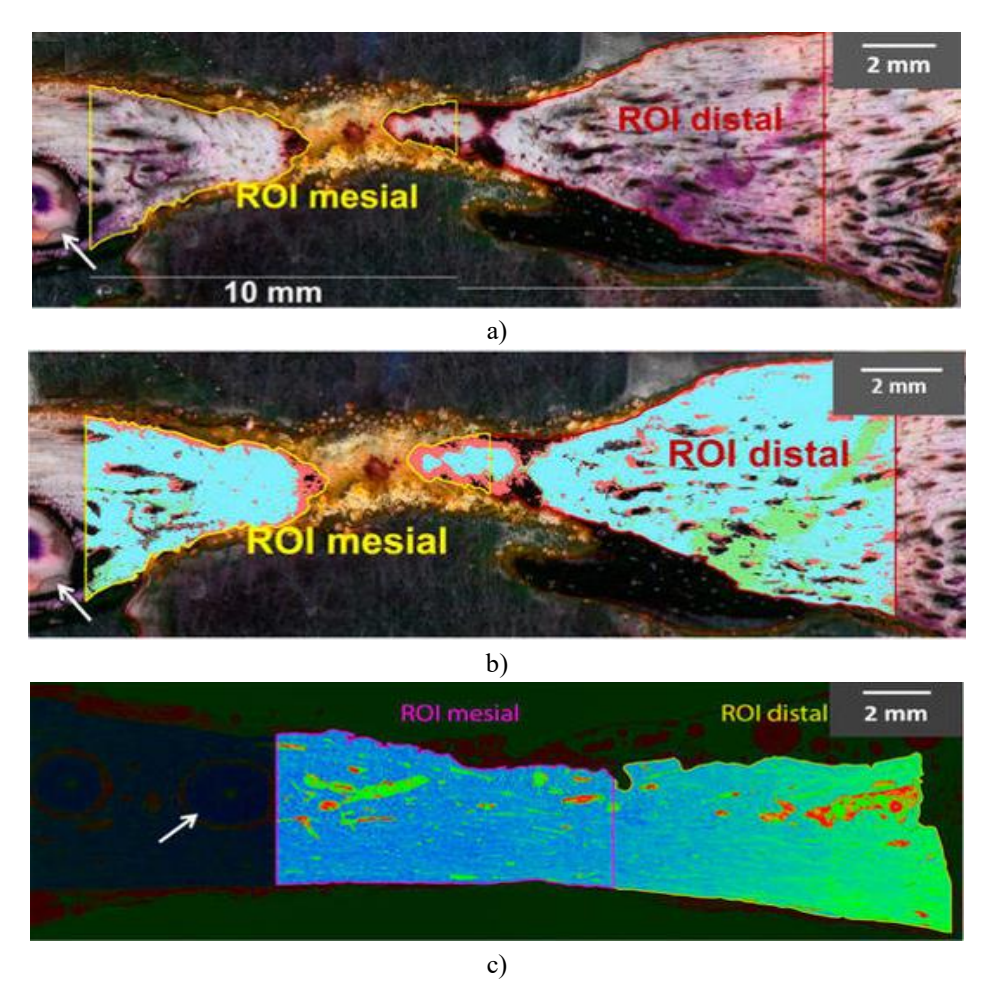


Figure 4. Light microscopy of a stained thin section showing the designated ROIs (a). Post-histomorphometric analysis, mineralized bone is highlighted in light blue, osteoid/cartilage in green, and bone marrow in red (b). Scanning acoustic microscopy (c) illustrates the same section with marked ROIs, with arrows indicating the PM2 roots within the augmented defects.

For light microscopy image processing, Olympus cellSens Dimension V1.8.1 software (Olympus Germany, Hamburg) was used to assemble composite

images from multiple captures. Both LM and SAM analyses were employed.

Statistical analysis

All datasets were analyzed using GraphPad Prism 6.01 (GraphPad Software, La Jolla, CA, USA). Descriptive statistics, including mean values and standard deviations, were calculated. Normality was assessed via the Shapiro–Wilk test. Due to the non-parametric nature of the variables, differences between groups were analyzed using the Wilcoxon–Mann–Whitney test. Statistical significance was defined as $p \leq 0.05$.

Results and Discussion

All surgical procedures were completed successfully, and the dogs tolerated a soft diet from the day of surgery onward. Healing proceeded smoothly, with no complications directly linked to the critical-sized defects. However, 21 days after surgery, Dog 1 suffered a spontaneous mandibular fracture, which prevented normal feeding, and was promptly euthanized.

Macroscopic and radiographic findings

No visible residual defects were detected on clinical inspection in any of the remaining dogs, regardless of the type of bone replacement material (BRM) applied. Radiographic assessment provided more detailed observations (Figure 5). Overall, none of the jaws displayed remaining BRM particles, indicating successful bone remodeling.

In Dog 2, the left mandible (augmented with nanocrystalline HA) showed a break in the crestal cortical bone, whereas the right side (augmented with bovine XENO) exhibited a greater amount of bone above the mandibular canal. For Dog 3, the alveolar bone level on the left side (AUTO) was higher than the right side (XENO), and an encapsulated root fragment was noted on the right. Dog 4 had a higher alveolar bone level on the left side (AUTO) compared with the right side (HA), especially above the mandibular canal. Radiographically, the autogenous bone regions (AUTO) in Dogs 3 and 4 (left side) appeared similar, whereas the right side of Dog 4 resembled the XENO-augmented area in Dog 3 in terms of bone density.

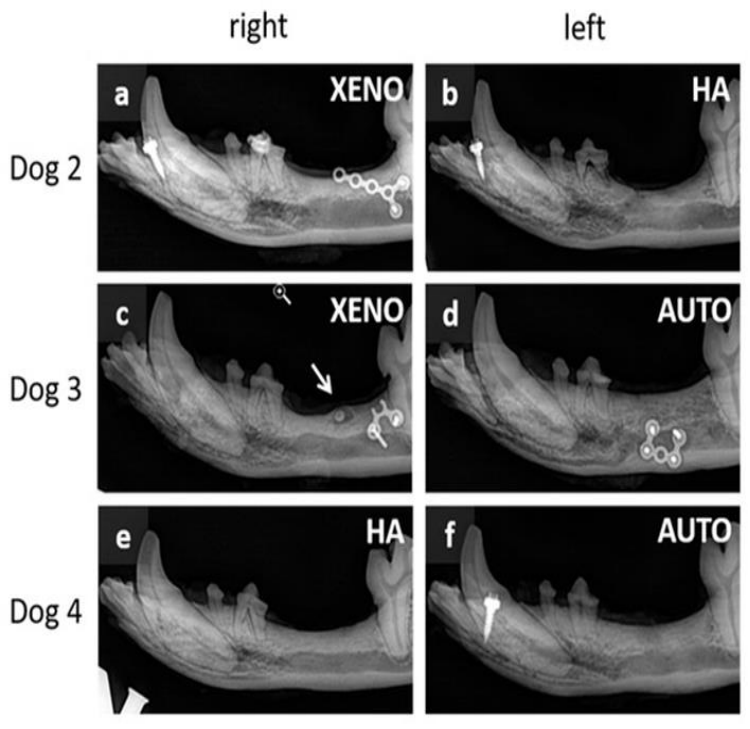


Figure 5. Radiographs of resected mandibles 30 weeks after implantation: (a, c, e) right sides of Dogs 2, 3, and 4; (b, d, f) left sides of Dogs 2, 3, and 4. XENO: xenograft; HA: hydroxyapatite; AUTO: autograft. No residual BRM material was observed. Arrows indicate encapsulated root fragments.

Periodontal ligament gap assessment

To evaluate the effect of orthodontic forces on teeth adjacent to the augmented defects, PDL widths were measured. **Figure 6** presents LM images of PM1 along with the mesial and distal roots of PM2. The PDL surrounding PM1 was consistently smooth and evenly

distributed. In contrast, PM2 displayed markedly larger and irregular PDL gaps, with multiple protuberances along the root surfaces, highlighting uneven remodeling during orthodontic movement into the grafted critical-sized defects.

Pal et al., Periodontal Gap Dynamics after Prolonged Tooth Movement into Surgically Augmented Critical-Size Defects in Beagle Jaws

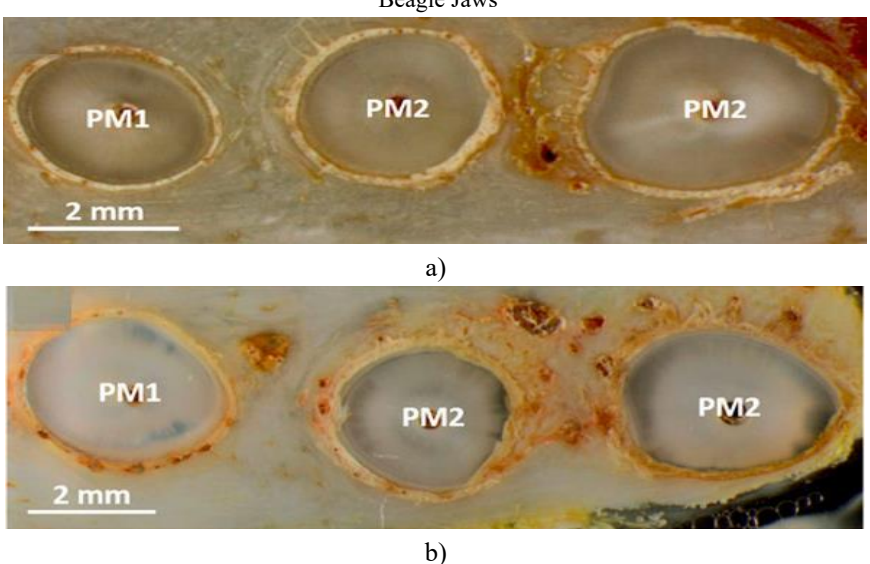


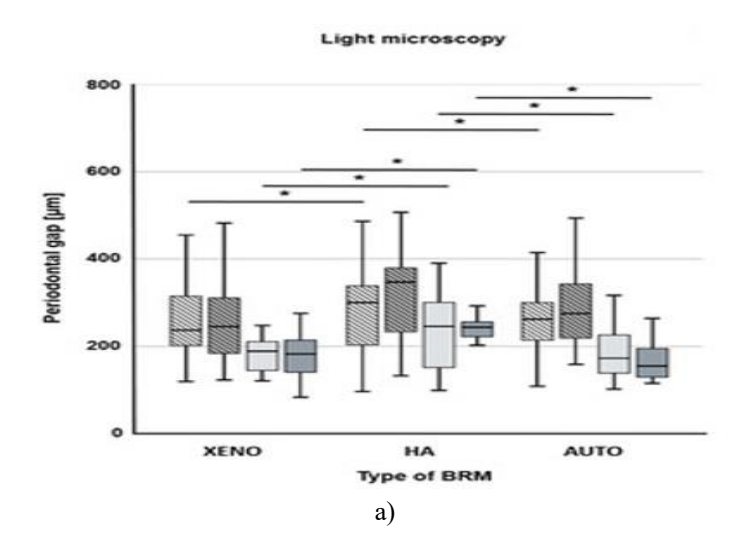
Figure 6. Representative LM images demonstrate the periodontal spaces of PM1 (single-rooted) and PM2 (mesial and distal roots): a) Dog 3, left mandible; b) Dog 2, right mandible. In both samples, PM1 displayed a narrow, smooth, and consistent periodontal gap, while PM2 exhibited enlarged and irregular spaces with multiple root-surface protrusions.

Regardless of graft type or root orientation (mesial vs. distal), LM analyses showed that compression-side gaps were consistently larger than those on the tension side (XENO: $0.25 \pm 0.09~\mu m$ vs. $0.19 \pm 0.05~\mu m$; HA: $0.31 \pm 0.13~\mu m$ vs. $0.23 \pm 0.09~\mu m$; C: $0.27 \pm 0.11~\mu m$ vs. $0.18 \pm 0.06~\mu m$; p ≤ 0.05) (Figure 7a). The same distribution was observed with SAM evaluation (XENO: $0.24 \pm 0.08~\mu m$ vs. $0.18 \pm 0.06~\mu m$; HA: $0.39 \pm 0.14~\mu m$ vs. $0.32 \pm 0.08~\mu m$; C: $0.27 \pm 0.10~\mu m$ vs. $0.17 \pm 0.04~\mu m$; p ≤ 0.05). When comparing mesial and distal roots of PM2, the gap dimensions were generally equivalent across sides, with the exception of HA in the mesial root under SAM, where no statistical significance was reached ($0.35 \pm 0.12~\mu m$ vs. $0.32 \pm 0.06~\mu m$; p = 0.22) (Figure 7b).

The biomaterial used affected gap size. XENO and AUTO showed comparable outcomes, whereas

nanocrystalline HA generated distinctly broader spaces, regardless of the imaging approach. In LM assessments, the distal root compression side revealed no statistical difference between HA and the other materials, yet the mesial root and both tension areas were significantly wider in HA groups ($p \le 0.05$). SAM confirmed this trend, with HA producing the largest measurements compared to XENO and AUTO across all root positions and sides ($p \le 0.05$).

Additionally, methodological variation was evident in HA cases. SAM consistently measured wider spaces than LM, both for the distal root compression side (LM: $0.30 \pm 0.12~\mu m$; SAM: $0.40 \pm 0.14~\mu m$; $p \le 0.05$) and for the mesial root tension side (LM: $0.23 \pm 0.09~\mu m$; SAM: $0.33 \pm 0.07~\mu m$; $p \le 0.05$).



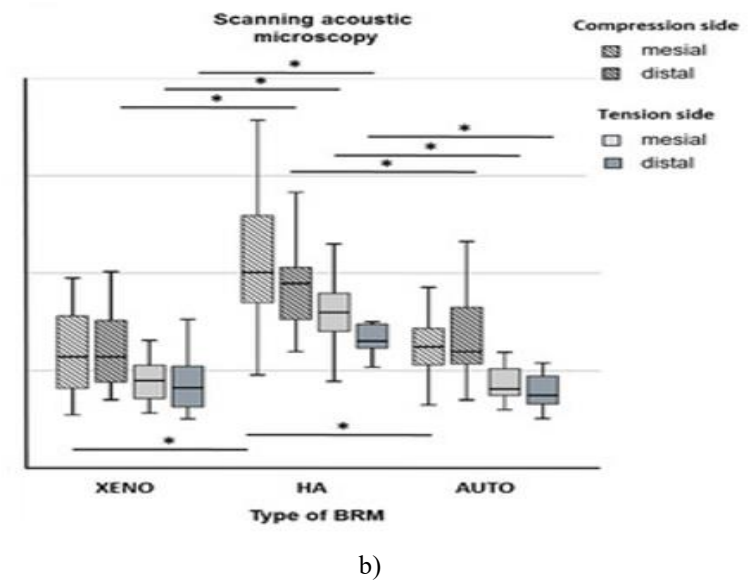


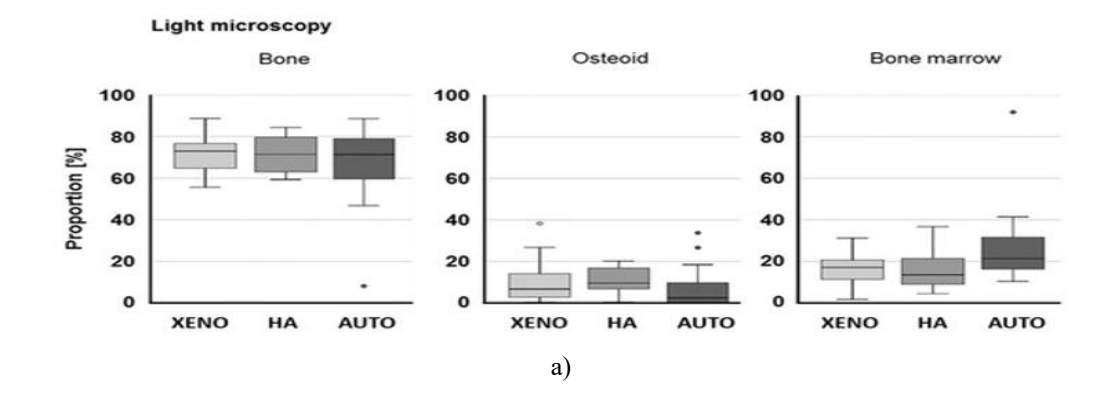
Figure 7. Mean values (± SD) of periodontal gap width for the mesial and distal roots of PM2 following orthodontic relocation into the reconstructed critical-sized defect. Assessments were carried out at three separate locations on both compression and tension surfaces, using light microscopy (a) and scanning acoustic microscopy (b). The mesial and distal roots were evaluated independently. Abbreviations: XENO = xenograft; HA = hydroxyapatite; AUTO = autograft. Asterisks (*) indicate statistically significant variations between BRMs (p ≤ 0.05).

Relative amounts of bone, osteoid, and bone marrow New bone formation was quantified by two imaging techniques: light microscopy (LM) and scanning acoustic microscopy (SAM) (Figure 8). Across all biomaterials, both analyses indicated that the fraction of bone marrow remained rather low (LM: $20.9 \pm 13.9\%$; SAM: $9.8 \pm 5.4\%$; $p \le 0.05$). A clear discrepancy between the two techniques appeared only for autograft (AUTO), with LM reporting $26.9 \pm 22.2\%$ and SAM showing $8.5 \pm 4.2\%$ ($p \le 0.05$).

Osteoid measurements also differed substantially between methods. LM revealed only $9.1 \pm 9.5\%$, whereas SAM produced a much larger proportion (29.4 \pm 19.4%; p \leq 0.05). When analyzed separately by biomaterial, LM consistently provided lower osteoid percentages than SAM (XENO: $10.1 \pm 11.5\%$ vs. 27.3

 \pm 13.3%; HA: 6.0 \pm 4.3% vs. 63.3 \pm 23.1%; AUTO: 4.8 \pm 9.5% vs. 20.3 \pm 9.5%; p \leq 0.05).

For mineralized bone, results from LM and SAM were comparable in the case of xenograft (XENO: 74.0 \pm 9.9% vs. 63.1 \pm 15.0%) and autograft (AUTO: 68.2 \pm 22.4% vs. 71.2 \pm 11.1%). However, nanocrystalline hydroxyapatite (HA) demonstrated a marked divergence between the two methods, with LM giving far higher values than SAM (75.5 \pm 10.3% vs. 22.1 \pm 27.5%; p \leq 0.05). The HA data from SAM were striking because of the unusually elevated osteoid proportion combined with a comparatively small quantity of mineralized bone, setting them apart from both XENO and AUTO, and also from the LM results for HA.



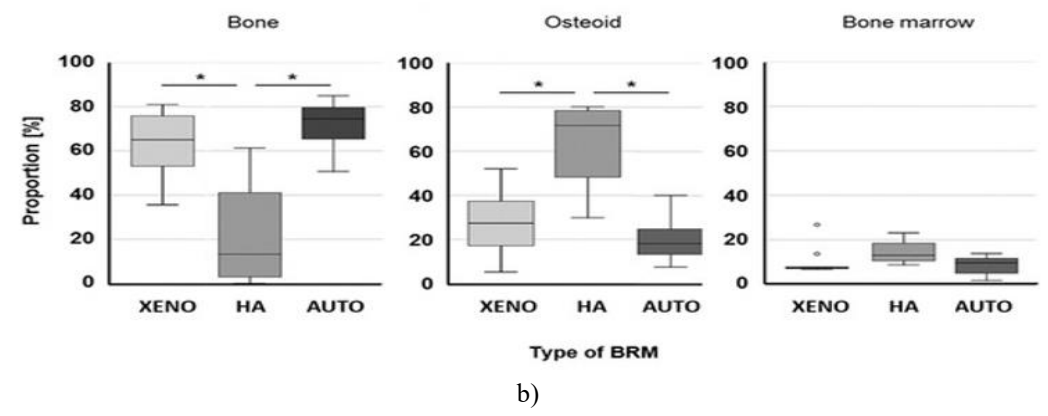


Figure 8. The mesial and distal ROIs were analyzed for the relative shares of bone, osteoid, and bone marrow, with results displayed as boxplots. Panel (a) illustrates outcomes obtained through light microscopy, while panel (b) represents findings from scanning acoustic microscopy. AUTO = autograft; HA = hydroxyapatite; XENO = xenograft. Statistically meaningful variations are denoted by an asterisk (p ≤ 0.05).

This investigation in beagle dogs focused on alterations in the width and morphology of the periodontal ligament (PDL) surrounding the roots of the second premolars, which were orthodontically displaced into critical-sized defects previously augmented with various bone replacement materials (BRMs). Autogenous bone grafts, considered the clinical gold standard, served as the control. Utilizing BRMs as substitutes for autogenous bone in critical-sized defects could be especially valuable in maxillofacial surgery, for instance in patients with cleft lip, alveolus, or palate, who may require alveolar bone augmentation before adjacent teeth can be moved into the reconstructed region.

All surgical procedures in the animals were completed without intraoperative complications, and post-surgical recovery proceeded uneventfully. The cause of the mandibular fracture observed in Dog 1 overnight remains unclear. Due to this fracture, the dog could no longer feed normally and had to be euthanized. Such fractures are likely related to the weakened bone structure inherent to critical-sized defects.

As anticipated, defects augmented with autogenous bone demonstrated effective healing. Previous studies have also highlighted the advantages of autologous bone in repairing large bony defects, not only in dental but also in broader surgical contexts [20, 21]. The BRMs used in this study, including bovine xenograft and nanocrystalline hydroxyapatite (HA), have shown satisfactory performance in earlier research. Radiographic outcomes from the current study align with previous reports supporting the suitability of these materials for bone augmentation [22-27]. Their use prior to orthodontic tooth movement (OTM) has been demonstrated in multiple studies [28-32], although most of those investigations involved extraction sockets rather than critical-sized defects. In those studies, neighboring teeth could successfully be moved into the augmented sites.

While the present measurements did not directly quantify OTM, the observed changes in PDL dimensions on compression and tension sides suggest that applied forces during tooth movement initiate bone resorption and formation, facilitating Histomorphometric analyses (Figure 8) confirmed functional bone formation. However, in defects augmented with nanocrystalline HA, the newly formed bone was particularly dense, which correlated with root resorption of PM2 in both jaws treated with HA. From orthodontic perspective, this indicates that nanocrystalline HA may not be optimal for augmenting critical-sized defects prior to tooth movement.

A study by Seifi et al. [31] in dogs reported no significant differences in root resorption between HAfilled and non-intervened artificial sockets; however, even the untreated group exhibited nearly 20% root resorption in the mandible after 2 months. Direct comparison is limited, likely due to differences in HA form-granules in Seifi et al. versus blocks in the present study-which may induce distinct cellular responses. Troedhan et al. [23] observed that insertion torque values for dental implants were substantially higher in nanocrystalline HA compared to bovine xenografts, suggesting that OTM may face greater resistance in HA-augmented defects, thus increasing the risk of root resorption. Gao et al. [33] emphasized that inconsistencies in the relationship between bone density and root resorption warrant investigation.

This investigation revealed that the periodontal ligament (PDL) reacts distinctly to orthodontic forces when different graft materials—XENO and HA—are used. PDL measurements indicated reduced widths on the tension side for AUTO, XENO, and HA, whereas

nanocrystalline HA displayed notably larger gaps in both light microscopy (LM) and scanning acoustic microscopy (SAM) analyses (Figure 7). The experimental setup does not permit direct conclusions about the interplay between bone formation and resorption. Nonetheless, the variation in PDL widths on compression and tension sides indicates that orthodontic tooth movement (OTM) occurred under the applied forces. Based on previous literature, the OTM in this study likely progressed over six months [28, 31, 32]. Tanimoto *et al.* and Abe *et al.* documented approximately 6 mm of tooth displacement after 6 months using carbonated HA alone or combined with deproteinized bovine bone mineral (BioOss®, XENO) [28, 32].

Mechanical loading of teeth initiates OTM through an aseptic inflammatory response [1, 2, 4], activating a complex cascade of cellular events. According to the Biphasic Theory [2], adapted from the pressuretension concept [4], these events occur simultaneously on both the compression and tension sides. As described by Alikhani *et al.* "the Catabolic Phase precedes the Anabolic Phase, with specific cellular and molecular mechanisms delineating the transition between phases" [2]. Consequently, the PDL gap enlarges on the compression side while narrowing on the tension side, facilitating tooth movement in the direction of force.

PDL measurements in this study support this framework, showing the expected configuration nearly six months after applying orthodontic force. Compared with the early days following force initiation, the PDL undergoes substantial remodeling over time. Previous studies analyzing the first 3–14 days after tooth movement observed PDL compression on the pressure side with narrowing, and widening on the tension side [10, 13, 15]. In the present experiment, continuous force application resulted in wider PDL gaps on the compression side relative to the tension side, indicating that bone remodeling had reached a steady state, consistent with the Biphasic Theory [2]. Had equilibrium not been achieved, a narrower PDL gap would still have been present on the compression side.

Conclusion

This investigation presents the first long-term evaluation of alterations in the dimensions and morphology of the periodontal ligament space in teeth moved into critical-sized defects after augmentation with different bone replacement materials. The results offer novel and complementary insights into bone remodeling associated with orthodontic tooth movement in extensively augmented regions. Due to

the limited number of animals included, these findings should be interpreted with caution. Preliminary observations suggest that over several months, the compression side may not conform to the traditional behavior described in the pressure—tension theory [4]. Additional studies are necessary to fully elucidate the temporal patterns and mechanisms underlying these changes.

Acknowledgments: None

Conflict of Interest: None

Financial Support: None

Ethics Statement: None

References

- Li Y, Zhan Q, Bao M, Yi J, Li Y. Biomechanical and biological responses of periodontium in orthodontic tooth movement: update in a new decade. Int J Oral Sci. 2021;13(1):20.
- Alikhani M, Sangsuwon C, Alansari S, Nervina JM, Teixeira CC. Biphasic theory: breakthrough understanding of tooth movement. J World Fed Orthod. 2018;7(3):82–8.
- Nakamura Y, Tanaka T, Noda K, Shimpo S, Oikawa T, Hirashita A, et al. Calcification of degenerating tissues in the periodontal ligament during tooth movement. J Periodontal Res. 2003;38(3):343–50.
- 4. Krishnan V, Davidovitch Z. Cellular, molecular, and tissue-level reactions to orthodontic force. Am J Orthod Dentofac Orthop. 2006;129(4):469-e1.
- Tsuge A, Noda K, Nakamura Y. Early tissue reaction in the tension zone of PDL during orthodontic tooth movement. Arch Oral Biol. 2016;65:17–25.
- Zong C, van Dessel J, Vande Velde G, Willems G, Cadenas de Llano-Pérula M. Dynamic changes in tooth displacement and bone morphometry induced by orthodontic force. Sci Rep. 2022;12(1):13672.
- 7. Aveic S, Craveiro RB, Wolf M, Fischer H. Current trends in in vitro modeling to mimic cellular crosstalk in periodontal tissue. Adv Healthc Mater. 2021;10(1):e2001269.
- Meikle MC. The tissue, cellular, and molecular regulation of orthodontic tooth movement: 100 years after Carl Sandstedt. Eur J Orthod. 2006;28(3):221-40.
- Rizk M, Niederau C, Florea A, Kiessling F, Morgenroth A, Mottaghy FM, et al. Periodontal

- ligament and alveolar bone remodeling during long orthodontic tooth movement analyzed by a novel user-independent 3D-methodology. Sci Rep. 2023;13(1):19919.
- Shalish M, Will LA, Fukai N, Hou B, Olsen BR. Role of polycystin-1 in bone remodeling: orthodontic tooth movement study in mutant mice. Angle Orthod. 2014;84(5):885–90.
- 11. Ru N, Liu SSY, Zhuang L, Li S, Bai Y. In vivo microcomputed tomography evaluation of rat alveolar bone and root resorption during orthodontic tooth movement. Angle Orthod. 2013;83(3):402–9.
- 12. Jeon HH, Yang CY, Shin MK, Wang J, Patel JH, Chung CH, et al. Osteoblast lineage cells and periodontal ligament fibroblasts regulate orthodontic tooth movement dependent on NF-κB activation. Angle Orthod. 2021;91(5):664–71.
- 13. Mena Laura EE, Cestari TM, Almeida R, Pereira DS, Taga R, Garlet GP, et al. Metformin as an addon to insulin improves periodontal response during orthodontic tooth movement in type 1 diabetic rats. J Periodontol. 2019;90(8):920–31.
- 14. Li H, Xia L, Wang S, Al-Balaa M, Liu W, Hua X. Expression of extracellular matrix metalloproteinase inducer (EMMPRIN) in the compression area during orthodontic relapse. Eur J Orthod. 2020;42(3):347–54.
- Nakamura Y, Noda K, Shimoda S, Oikawa T, Arai C, Nomura Y, et al. Time-lapse observation of rat periodontal ligament during function and tooth movement using microcomputed tomography. Eur J Orthod. 2008;30(3):320–6.
- Sun J, Zhang X, Li R, Chen Z, Huang Y, Chen Z. Biological effects of orthodontic tooth movement into the grafted alveolar cleft. J Oral Maxillofac Surg. 2018;76(3):605–15.
- 17. Ru N, Liu SSY, Bai Y, Li S, Liu Y, Wei X. BoneCeramic graft regenerates alveolar defects but slows orthodontic tooth movement with less root resorption. Am J Orthod Dentofac Orthop. 2016;149(4):523–32.
- 18. Möhlhenrich SC, Kniha K, Magnuska Z, Chhatwani S, Hermanns-Sachweh B, Gremse F, et al. Development of root resorption during orthodontic tooth movement after cleft repair using different grafting materials in rats. Clin Oral Investig. 2022;26(9):5809–21.
- 19. Nauth A, Schemitsch E, Norris B, Nollin Z, Watson JT. Critical-size bone defects: Is there a consensus for diagnosis and treatment? J Orthop Trauma. 2018;32(Suppl 1):S7–11.

- 20. Cabbad NC, Stalder MW, Arroyave A, Wolfe EM, Wolfe SA. Autogenous bone cranioplasty: review of a 42-year experience by a single surgeon. Plast Reconstr Surg. 2019;143(6):1713–23.
- Fearon JA, Griner D, Ditthakasem K, Herbert M. Autogenous bone reconstruction of large secondary skull defects. Plast Reconstr Surg. 2017;139(2):427–38.
- 22. Liu Q, Douglas T, Zamponi C, Becker ST, Sherry E, Sivananthan S, et al. Comparison of in vitro biocompatibility of NanoBone® and BioOss® for human osteoblasts. Clin Oral Implant Res. 2011;22(11):1259–64.
- 23. Troedhan A, Schlichting I, Kurrek A, Wainwright M. Primary implant stability in augmented sinuslift sites after completed bone regeneration: a randomized controlled clinical study comparing four subantral biomaterials. Sci Rep. 2014;4(1):5877.
- 24. Zhang Y, Al-Maawi S, Wang X, Sader R, Kirkpatrick CJ, Ghanaati S. Biomaterial-induced multinucleated giant cells express proinflammatory signaling molecules: a histological study in humans. J Biomed Mater Res A. 2019;107(4):780–90.
- 25. Dau M, Kämmerer PW, Henkel KO, Gerber T, Frerich B, Gundlach KKH. Bone formation in monocortical mandibular critical-size defects after augmentation with two synthetic nanostructured and one xenogenous hydroxyapatite bone substitute: an in vivo animal study. Clin Oral Implant Res. 2016;27(5):597–603.
- 26. Kijartorn P, Wongpairojpanich J, Thammarakcharoen F, Suwanprateeb J, Buranawat B. Clinical evaluation of 3D printed nanoporous hydroxyapatite bone graft for alveolar ridge preservation: a randomized controlled trial. J Dent Sci. 2022;17(1):194–203.
- 27. Wähnert D, Koettnitz J, Merten M, Kronenberg D, Stange R, Greiner JFW, et al. SpongostanTM leads to increased regeneration of a rat calvarial critical-size defect compared to NanoBone® and Actifuse. Materials. 2021;14(8):1961.
- 28. Tanimoto K, Sumi K, Yoshioka M, Oki N, Tanne Y, Awada T, et al. Experimental tooth movement into new bone area regenerated by use of bone marrow-derived mesenchymal stem cells. Cleft Palate Craniofac J. 2015;52(4):386–94.
- 29. Araújo MG, Carmagnola D, Berglundh T, Thilander B, Lindhe J. Orthodontic movement in bone defects augmented with Bio-Oss: an experimental study in dogs. J Clin Periodontol. 2001;28(1):73–80.

- 30. Machibya FM, Zhuang Y, Guo W, You D, Lin S, Wu D, et al. Effects of bone regeneration materials and tooth movement timing on canine experimental orthodontic treatment. Angle Orthod. 2018;88(2):171–8.
- 31. Seifi M, Arayesh A, Shamloo N, Hamedi R. Effect of nanocrystalline hydroxyapatite socket preservation on orthodontically induced inflammatory root resorption. Cell J. 2015;16(4):514–27.
- 32. Abe T, Kunimatsu R, Tanimoto K. Comparison of orthodontic tooth movement of regenerated bone induced by carbonated hydroxyapatite or deproteinized bovine bone mineral in beagle dogs. Materials. 2023;17(1):112.
- 33. Gao Y, Min Q, Li X, Liu L, Lv Y, Xu W, et al. Immune system acts on orthodontic tooth movement: cellular and molecular mechanisms. Biomed Res Int. 2022;2022(1):9668610.